The rough-wall turbulent boundary layer from the hydraulically smooth to the fully rough regime

M. P. SCHULTZ[1] AND K. A. FLACK[2]

[1]Naval Architecture and Ocean Engineering Department, United States Naval Academy, Annapolis, MD 21402, USA

[2]Mechanical Engineering Department, United States Naval Academy, Annapolis, MD 21402, USA

Turbulence measurements for rough-wall boundary layers are presented and compared to those for a smooth wall. The rough-wall experiments were made on a three-dimensional rough surface geometrically similar to the honed pipe roughness used by Shockling, Allen & Smits (*J. Fluid Mech.* vol. 564, 2006, p. 267). The present work covers a wide Reynolds-number range ($Re_\theta = 2180–27\,100$), spanning the hydraulically smooth to the fully rough flow regimes for a single surface, while maintaining a roughness height that is a small fraction of the boundary-layer thickness. In this investigation, the root-mean-square roughness height was at least three orders of magnitude smaller than the boundary-layer thickness, and the Kármán number (δ^+), typifying the ratio of the largest to the smallest turbulent scales in the flow, was as high as 10 100. The mean velocity profiles for the rough and smooth walls show remarkable similarity in the outer layer using velocity-defect scaling. The Reynolds stresses and higher-order turbulence statistics also show excellent agreement in the outer layer. The results lend strong support to the concept of outer layer similarity for rough walls in which there is a large separation between the roughness length scale and the largest turbulence scales in the flow.

1. Introduction

Understanding the effect of roughness on wall-bounded turbulence is of practical importance in the prediction of a wide range of industrial and geophysical flows. Examples range from flow through pipes and over vehicles to atmospheric boundary layers. Seminal work in this area was carried out by Nikuradse (1933) and Colebrook & White (1937). While this work focused on roughness effects on the mean flow and wall shear stress, later studies investigated the effect of roughness on the turbulence structure (e.g. Perry & Joubert 1963; Perry, Schofield & Joubert 1969; Antonia & Luxton 1971; Ligrani & Moffat 1986; Bandyopadhyay 1987; Krogstad, Antonia & Browne 1992). An extensive review of the literature on rough-wall boundary layers was given by Raupach, Antonia & Rajagopalan (1991). An important conclusion of their work was that there is strong experimental evidence of outer-layer similarity in the turbulence structure over smooth and rough walls. This is termed the 'wall similarity' hypothesis, and it states that at high Reynolds number, turbulent motions are independent of wall roughness and viscosity outside the roughness sublayer

(or viscous sublayer in the case of a smooth wall). The roughness sublayer is the region directly above the roughness extending about $5k$ from the wall (where k is the roughness height) in which the turbulent motions are directly influenced by the roughness length scales. Raupach *et al.* (1991) noted that the wall similarity hypothesis is an extension of Townsend's (1976) concept of Reynolds-number similarity for turbulent flows.

Since Raupach *et al.*'s review, the concept of wall similarity has come into question. Experimental studies of rough-wall boundary layers by Krogstad *et al.* (1992), Tachie, Bergstrom & Balachandar (2000) and Keirsbulck *et al.* (2002) have all observed significant changes to the Reynolds stresses that extend well into the outer layer for flows over woven mesh and transverse bar roughness. Numerical simulations of turbulent channel flow by Leonardi *et al.* (2003) and Bhaganagar, Kim & Coleman (2004) also show that roughness effects can be observed in the outer layer. However, the experimental studies of Kunkel & Marusic (2006) and the present authors (Flack, Schultz & Shapiro 2005) provide support for wall similarity in smooth- and rough-wall boundary layer in terms of both the mean flow and the Reynolds stresses. The work of Kunkel & Marusic (2006) is notable because of the extremely high Reynolds number and large separation of scales in the turbulent boundary layers that were studied.

Jiménez (2004) states that the conflicting views regarding the validity of the wall similarity hypothesis may be due to the effect of the relative roughness, k/δ, on the flow (where δ is the boundary-layer thickness). Jiménez concluded that if the roughness height is small compared the boundary-layer thickness ($k/\delta < 1/50$), the effect of the roughness should be confined to the inner layer and wall similarity will hold. If, on the other hand, the roughness height is large compared to the boundary-layer thickness ($k/\delta \geqslant 1/50$), roughness effects on the turbulence may extend across the entire boundary layer, and the concept of wall similarity will be invalid. However, Jiménez (2004) notes that the classical notion of wall similarity has implications far beyond roughness studies, extending to the fundamental concepts of turbulence modelling. For example, the underpinning of large-eddy simulation (LES) is that the small turbulence scales have little influence on the large energy-containing scales. If surface roughness exerts an influence across the entire boundary layer, this may not be a valid assumption.

In view of the conflicting evidence regarding the wall similarity hypothesis, the purpose of the present study was to assess its validity when the criteria for similarity are strictly adhered to, that is, the Reynolds number is sufficiently high and the roughness is small compared to the boundary-layer thickness. It would seem that wall similarity for larger relative roughness cannot be expected if it does not hold true for the limiting case. In this study, the structure of the rough-wall boundary layer in terms of the mean flow, Reynolds stresses and higher-order turbulence statistics is compared with that for a smooth wall. The present work covers a wide Reynolds-number range, spanning the hydraulically smooth to the fully rough flow regime for a single surface, while maintaining a roughness height that is a small fraction of the boundary-layer thickness. To our knowledge, the present paper documents the turbulence quantities of a rough-wall boundary layer at the highest Reynolds number ($Re_\theta = 27\,080$) reported in the literature from a laboratory study. The studies of Andreopoulos & Bradshaw (1981) at $Re_\theta \sim 20\,000$ and Ligrani & Moffat (1986) at $Re_\theta \leqslant 18\,700$ mark the largest Reynolds numbers previously studied; however, in both these studies, the ratio k/δ was much larger than in the present work.

2. Background

2.1. *Mean flow*

The flow in a turbulent boundary layer can be broken into two regions: the inner and outer layers, each having its own scaling. In the inner layer, the mean velocity, U, at a given distance from the wall, y, is determined by the friction velocity, U_τ, the kinematic viscosity, ν, and the roughness height, k, such that (Schubauer & Tchen 1961)

$$U = f_1(y, U_\tau, \nu, k). \tag{2.1}$$

In non-dimensional form this is the 'law of the wall', given as

$$U^+ = f(y^+, k^+) \tag{2.2}$$

where $U^+ = U/U_\tau$, $y^+ = yU_\tau/\nu$, $k^+ = kU_\tau/\nu$, $U_\tau = (\tau_w/\rho)^{1/2}$, τ_w is the wall shear stress, and ρ is the fluid density. In the outer region, the difference between the velocity at the outer edge of the boundary-layer, U_e, and the local mean velocity, U, at a distance y from the wall is determined by the boundary-layer thickness, δ (δ is understood to be δ_{99}, the distance from the wall where the mean velocity is $0.99U_e$) and U_τ, such that (von Kármán 1930)

$$U_e - U = g_1(y, \delta, U_\tau). \tag{2.3}$$

In non-dimensional form this is the 'velocity-defect law', given as

$$U_e^+ - U^+ = g(\eta), \tag{2.4}$$

where $U_e^+ = U_e/U_\tau$ and $\eta = y/\delta$.

Millikan (1938) proposed, by matching the velocity profiles in the law of the wall (equation (2.2)) and the velocity-defect law (equation (2.4)), that a logarithmic velocity distribution results in the overlap region ($\delta \gg y \gg \nu/U_\tau$) at sufficiently high Reynolds number. This is the 'log-law' and for a smooth-wall turbulent boundary layer, is given by

$$U^+ = \frac{1}{\kappa} \ln(y^+) + B, \tag{2.5}$$

where the von Kármán constant $\kappa \approx 0.421$ and the smooth-wall log-law intercept $B \approx 5.60$ (McKeon *et al.* 2004). The 'log-law' can also be expressed in velocity-defect form as

$$U_e^+ - U^+ = -\frac{1}{\kappa} \ln(\eta) + B_1, \tag{2.6}$$

where B_1 is the velocity-defect intercept ($2\Pi/\kappa$) and Π is the wake strength.

Clauser (1954) and Hama (1954) found that the effect of surface roughness on the mean flow was confined to the inner layer, causing a downward shift in the log-law (equation (2.5)) called the roughness function, ΔU^+. Equation (2.5) can, therefore, be recast for rough-wall boundary layers as

$$U^+ = \frac{1}{\kappa} \ln(y^+) + B - \Delta U^+. \tag{2.7}$$

Coles (1956) extended (2.7) to cover both the overlap and outer region of the boundary layer using the wake function, ω. This is the 'law of the wake'. For smooth- and rough-wall boundary layers, it is as follows:

$$U^+ = \frac{1}{\kappa} \ln(y^+) + B + \frac{\Pi}{\kappa} \omega(\eta) \quad \text{(smooth wall)}, \tag{2.8}$$

$$U^+ = \frac{1}{\kappa}\ln(y^+) + B - \Delta U^+ + \frac{\Pi}{\kappa}\omega(\eta) \quad \text{(rough wall)}. \tag{2.9}$$

Turbulence models for Reynolds-averaged Navier–Stokes (RANS) computations usually account for roughness effects using the roughness function, ΔU^+ for the surface of interest (Patel 1998). They assume that the shape of the mean profile in the overlap and outer region for smooth and rough walls is the same as the smooth wall with the rough-wall profile being displaced by ΔU^+ below it. This is supported by the classic works of Clauser (1954) and Hama (1954) who observed that mean velocity in the outer region expressed in velocity-defect form ((2.4) and (2.6)) was independent of surface roughness. Using the wake function, velocity-defect scaling can be extended to describe the overlap and outer region of the boundary layer for both smooth- and rough-wall boundary layers as

$$U_e^+ - U^+ = -\frac{1}{\kappa}\ln(\eta) + B_1 - \frac{\Pi}{\kappa}\omega(\eta). \tag{2.10}$$

While many studies support a universal velocity-defect profile for smooth and rough walls, some have reported that Π is significantly increased for rough-wall flows (e.g. Krogstad *et al.* 1992; Tachie *et al.* 2000; Keirsbulck *et al.* 2002). This implies that the classic way of accounting for roughness effects on the mean flow through ΔU^+ may be misguided. Krogstad *et al.* (2005) provides support for a universal velocity-defect profile in fully developed turbulent channel flow using both experiment and direct numerical simulation. They maintain that the differences observed between boundary-layer and channel flows may be the result of the lack of a rotational–irrotational interface at the outer part of the shear layer in fully developed channel flow. Strong evidence of a universal velocity-defect profile for fully developed turbulent pipe flow was shown by Shockling, Allen & Smits (2006), who found that smooth and rough walls display similarity in the mean flow over a very large Reynolds number range.

2.2. *Turbulence quantities*

According to the wall similarity hypothesis, the energy-containing turbulent motions in a boundary layer are independent of roughness and viscosity at a sufficient distance from the wall except for the role they play in setting the boundary conditions for the outer flow (i.e. the velocity and length scales, U_τ and δ). Wall similarity can also be expressed in terms of the covariance of the velocity as

$$\overline{u_i'(y)u_j'(y + r)} = U_\tau^2 R_{ij}(y, \mathbf{r}; \delta), \tag{2.11}$$

where $\mathbf{r}$ is the separation vector, as long as the Reynolds number is sufficiently high and both y and $y + r$ are located outside the roughness sublayer (Raupach *et al.* 1991). This implies that single-point turbulence measurements (i.e. $\mathbf{r} \equiv \mathbf{0}$) over rough and smooth walls, such as the Reynolds stresses and higher-order turbulence statistics, should agree when scaled on outer variables. The studies of Raupach (1981), Perry & Li (1990), Ligrani & Moffat (1986), Kunkel & Marusic (2006) and the present authors (Schultz & Flack 2003; Flack *et al.* 2005) all show support for this. However, several studies have concluded that wall similarity is not valid for rough-wall flows (e.g. Krogstad *et al.* 1992; Keirsbulck *et al.* 2002; Leonardi *et al.* 2003; Bhaganagar *et al.* 2004).

Although there is general consensus in the literature that the streamwise Reynolds normal stress $(\overline{u'^2}^+)$ displays reasonable similarity in the outer flow with the exception of a few studies (e.g. Tachie *et al.* 2000), the effect on the wall-normal Reynolds normal stress $(\overline{v'^2}^+)$ and Reynolds shear stress $(-\overline{u'v'}^+)$ is not as clear. Krogstad *et al.*

Wall surface	U_τ (m s^{-1})	Re_θ	U_τ Clauser chart (m s^{-1})	U_τ Total stress (m s^{-1})	δ (mm)	δ^+	k_s^+	ΔU^+
Smooth	1.00	3110	0.0405	0.0394	29.0	1150	–	–
Smooth	5.00	13 140	0.181	0.182	26.3	4760	–	–
Rough	0.69	2175	0.0295	0.0289	29.2	843	2.3	0
Rough	1.00	3175	0.0415	0.0405	28.9	1180	3.2	0.14
Rough	3.00	8450	0.119	0.117	27.1	3150	9.2	1.5
Rough	5.00	13 800	0.202	0.199	25.5	5120	16	3.0
Rough	7.02	21 360	0.285	0.281	27.6	8030	23	4.2
Rough	7.96	27 080	0.322	0.320	31.2	10 100	26	4.6

TABLE 1. Experimental test conditions.

(1992) found significant increases in both $\overline{v'^2}^+$ and $-\overline{u'v'}^+$ for rough walls outside the roughness sublayer, with $\overline{v'^2}^+$ being affected most. Quadrant decomposition showed that the contribution to the Reynolds shear stress from $Q4$ events (i.e. sweeps) was increased close to the rough wall. This was attributed to the less strict boundary condition on v at $y = 0$ in the rough-wall case. The rough-wall v' spectra in the outer flow also exhibited significant differences across the entire wavenumber range. This result implies that the 'active' motions (i.e. the turbulence that contributes to the Reynolds shear stress) are not as universal as generally thought, and the 'inactive' motions, which are associated with larger-scale meandering motions in planes parallel to the wall, show a higher degree of similarity than the active motions.

Andreopoulos & Bradshaw (1981) showed that the velocity triple products involving v' are a sensitive indicator of changes in turbulence structure due to wall condition. They observed changes in the v' triple products out to $\sim 10k$ from a rough wall. Flack *et al.* (2005) found that the velocity triple products were nearly the same over smooth and rough walls beyond $5k$, giving support to the concept of wall similarity. Unfortunately, few other rough-wall studies, with the exception of Bandyopadhyay & Watson (1988), Antonia & Krogstad (2001) and Keirsbulck *et al.* (2002), have presented these statistics. This is mainly due to their inherently high experimental uncertainty.

3. Experiment

The experiments were conducted in the US Naval Academy's large re-circulating water tunnel. The test section of the tunnel is 40 cm × 40 cm in cross-section and is 1.8 m in length, with a tunnel velocity range of 0–8.0 m s^{-1} and a free-stream turbulence intensity of $\sim 0.5\%$. The current tests were run at six speeds within this range, producing a wide variation in Reynolds number ($Re_\theta = 2180$–27 100). The experimental test conditions are given in table 1. The test plates were flush mounted into a permanent splitter-plate test fixture. The test fixture was mounted horizontally, at mid-depth in the tunnel. The first 200 mm of the test fixture is covered with no. 36-grit sandpaper to ensure adequate turbulent boundary-layer tripping. Measurements were obtained 1.35 m downstream of the leading edge, allowing for a sufficient boundary-layer growth. Profiles taken from 0.90 m to the measurement location confirmed that the mean flow had reached self-similarity as witnessed by the collapse of the streamwise velocity-defect profiles. The upper removable wall of the tunnel is adjustable to account for boundary-layer growth. In the present work, the wall was set to produce a nearly zero pressure gradient boundary layer as witnessed by the acceleration parameter (K)
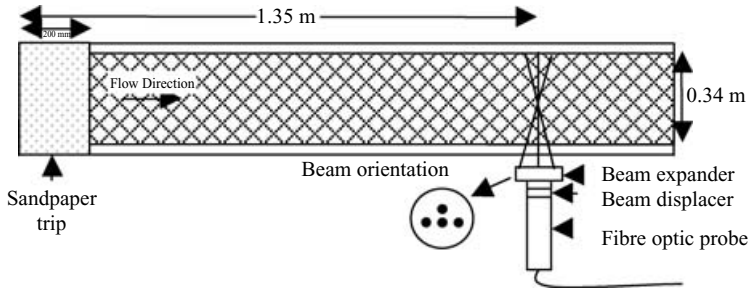
FIGURE 1. Experimental set-up.

which was $\leqslant 1 \times 10^{-8}$ in all test cases. The acceleration parameter is defined as

$$K = \frac{\nu}{U_e^2} \frac{\mathrm{d}U_e}{\mathrm{d}x}. \qquad (3.1)$$

Figure 1 shows a plan view of the flat-plate test fixture. Additional details of the experimental facility can be found in Schultz & Flack (2003) and Flack *et al.* (2005).

Two test plates were used in the current study; one smooth and one rough surface. The smooth surface was made of cast acrylic; the rough surface was produced by bi-directional sanding of a cast acrylic plate coated with silica-filled polyamide epoxy. A sanding block covered with no. 12-grit floor sanding paper was used to create linear scratches in the surface. Care was taken to sand using only linear motions across the test plate at an angle of $\pm 60°$ to the flow direction. The angle of the sanding was controlled using a guide template that was moved down the test plate. Sanding passes were first made at $+60°$ to the flow along the entire test plate and then the process was repeated at $-60°$ to the flow. The resulting roughness was a series of bi-directional scratches forming a diamond-shaped pattern. The process was developed to create a geometrically similar surface to the honed pipe roughness tested in the Princeton Superpipe facility (Shockling *et al.* 2006), since the honing process cannot be carried out on flat surfaces.

The surface roughness profiles of the test plates were measured using a Cyber Optics laser diode point range sensor laser profilometer system mounted to a Parker Daedal two-axis traverse with a resolution of $5\,\mu\mathrm{m}$. The resolution of the sensor is $1\,\mu\mathrm{m}$ with a laser spot diameter of $10\,\mu\mathrm{m}$. Data were taken over a sampling length of $50\,\mathrm{mm}$ and were digitized at a sampling interval of $25\,\mu\mathrm{m}$. Five linear profiles were taken on the rough surface in order to calculate statistics. A two-dimensional survey was also taken over a $5\,\mathrm{mm} \times 5\,\mathrm{mm}$ sampling area in order to document the surface topography (figure 2a). No filtering of the profiles was conducted except to remove any linear trend in the trace. The probability density function (p.d.f.) for the surface roughness elevations is presented in figure 2(b). The surface has a nearly Gaussian p.d.f. with a root-mean-square height, k_{rms}, of $26.3\,\mu\mathrm{m}$. The skewness of the p.d.f. is -0.46 and the flatness is 3.59. The average maximum peak to trough roughness height, k_T, for the five profiles was $193\,\mu\mathrm{m}$. The honed pipe tested by Shockling *et al.* (2006) has $k_{rms} = 2.5\,\mu\mathrm{m}$, a skewness of 0.31, and a flatness of 3.43. For reference, the original 'smooth' superpipe has $k_{rms} = 0.15\,\mu\mathrm{m}$, a skewness of -0.31, and a flatness of 3.6. Therefore, the present roughness is geometrically similar to the pipe surfaces tested in the superpipe facility with a roughness height that is ~ 10 times larger than the honed Superpipe and ~ 175 times larger than the original superpipe.
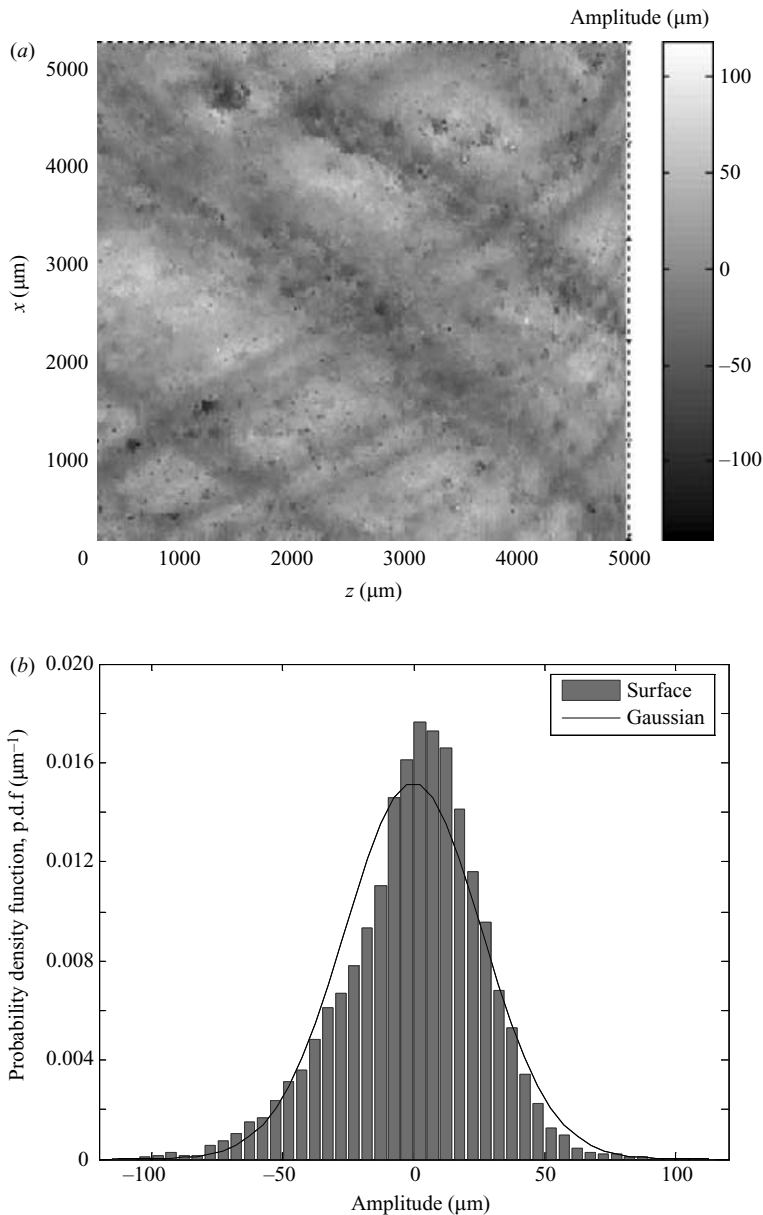
Figure 2. Test roughness: (*a*) surface elevation of roughness; (*b*) probability density function of roughness surface elevations.

Boundary-layer velocity measurements were obtained with a TSI FSA3500 two-component laser-Doppler velocimeter (LDV). The LDV consists of a four-beam fibre optic probe that collects data in backscatter mode. A custom designed beam displacer was added to the probe to shift one of the four beams, resulting in three co-planar beams that can be aligned parallel to the wall. This allowed for near-wall measurements without having to tilt the probe at a small angle or rotate the probe to resolve velocity components. Additionally, a 2.6:1 beam expander was located at the exit of the probe to reduce the size of the measurement volume. The resulting

probe volume diameter (d) was $45\,\mu\text{m}$ with a probe volume length (l) of $340\,\mu\text{m}$. The corresponding measurement volume diameter and length in viscous length scales ranged from $d^+ = 1.3$ and $l^+ = 10$ at the lowest Reynolds number to $d^+ = 15$ and $l^+ = 110$ at the highest Reynolds number. The small measurement volume diameter allowed for near-wall measurements, ($y^+ \approx 4$ for the lowest Reynolds number to $y^+ \approx 40$ for the highest Reynolds number) while assuring minimal velocity gradient bias due to finite probe diameter (Durst *et al.* 1998). The range of d^+ values in the present study is similar to the smooth-wall turbulent boundary layer study of DeGraaff & Eaton (2000). As opposed to hot-wire measurements (e.g. Johansson & Alfredsson 1983; Willmarth & Sharma 1984), the value of l^+ is not of critical importance for an LDV, since each individual velocity realization is for a single seeding particle in the probe volume. Therefore, each individual velocity realization is not spatially averaged. As long as the probe volume is aligned in a direction in which the turbulence quantities are homogeneous, the probe volume length will have no effect on the turbulence statistics. This was demonstrated by Luchik & Tiederman (1985) who measured turbulence quantities in a wall-bounded flow using LDV systems with $l^+ = 9$–74. They showed that there was no effect of l^+ on the measured streamwise root-mean-square velocity, and the turbulence measurements with an LDV system with this range of l^+ were at least as accurate as a hot wire with $l^+ = 0.5$. Although it cannot be ensured that the turbulence is entirely homogeneous in the spanwise direction, no significant differences were observed in the near-wall turbulence statistics when the probe was displaced by small distances in the spanwise direction.

A total of 40 000 random velocity samples were obtained at each location in the boundary layer. The data were collected in coincidence mode. The flow was seeded with $2\,\mu\text{m}$ alumina particles. The seed volume was controlled to achieve acceptable data rates while maintaining a low burst density signal (Adrian 1983). The probe was traversed to approximately 40 locations within the boundary layer with a Velmex three-axis traverse unit. The traverse allowed the position of the probe to be maintained to $\pm 5\,\mu\text{m}$ in all directions. The wall-normal velocity component was not obtained for the 8–10 data points closest to the wall owing to very low data rates and wall reflections.

Two methods were used to determine the friction velocity, U_τ, for both the smooth and rough surfaces (table 1). The first was the total stress method. It assumes a nominally constant shear stress region exists in the inner part of the boundary layer which is equal to the wall shear stress. The total stress was calculated at the plateau of the Reynolds shear stress profile in the overlap region of the boundary layer by summing the contributions of the viscous and turbulent stresses. The friction velocity, U_τ, was then calculated using the expression

$$U_\tau = \sqrt{\nu \frac{\partial U}{\partial y} - \overline{u'v'}}. \tag{3.2}$$

For the smooth wall, the friction velocity was also determined using the Clauser (1954) chart method, with log-law constants $\kappa = 0.421$ and $B = 5.6$ (McKeon *et al.* 2004). A modified Clauser chart method, described by Perry & Li (1990), was also employed to determine the friction velocity on the rough wall. The initial step in this process is to determine the wall datum offset using an iterative procedure. A plot of U/U_e versus $\ln(yU_e/\nu)$ was made for points in the log-law region (points between $y^+ = 100$, based on the value of U_τ obtained using the total stress method and $y/\delta = 0.125$). The wall normal distance is given as $y = y_T + \varepsilon$, where y_T is the

location of the top of the roughness elements, and ε is the wall datum offset. The wall datum offset is initially set to zero and then increased until the goodness-of-fit of a linear regression through the points is maximized. The wall datum offset in the present study was small ($\sim 50\,\mu\text{m}$) owing to the small roughness height. The friction velocity values obtained using the Clauser (smooth) and modified Clauser (rough) methods are used in the subsequent data reduction. It should be noted, however, that using U_τ determined from the total stress method would not change the trends in the presented results since the values obtained from both methods show good agreement. The difference between the two was $\leqslant 2.7\,\%$ in all cases, which is well within the uncertainty of the measurements. It should also be noted that values of U_τ for the smooth walls agree, within experimental uncertainty, with both the Re_θ-based correlation of Fernholz & Finley (1996), and the correlation of Österlund *et al.* (2000) which is based on direct measurement of the skin friction using oil-film interferometry.

Uncertainty estimates were obtained by combining both precision and bias errors, using the procedure described in Moffat (1988). The standard errors were determined from repeated velocity profiles taken on both the smooth and rough plates and 95 % confidence limits were determined from the Student's t-value, given by Coleman & Steele (1995). The precision uncertainties were obtained for the higher-order turbulence statistics using the bootstrap technique described in Efron (1982), since the statistical distribution of the parent population was not known *a priori*. The LDV data were corrected for velocity bias, described by Buchhave, George & Lumley (1979) by employing burst transit time weighting, and velocity gradient bias, detailed in Durst *et al.* (1998). Fringe bias was considered insignificant, as the beams were shifted well above a burst frequency representative of twice the free-stream velocity (Edwards 1987). Bias estimates were combined with the precision uncertainties to calculate the overall uncertainties for the measured quantities. The resulting overall uncertainty in the mean velocity is $\pm 1\,\%$. For the turbulence quantities $\overline{u'^2}$, $\overline{v'^2}$ and $\overline{u'v'}$, the overall uncertainties are $\pm 2\,\%$, $\pm 3\,\%$ and $\pm 5\,\%$, respectively. The uncertainty in U_τ for the smooth walls using the Clauser chart method is $\pm 3\,\%$, and the uncertainty in U_τ for the rough walls using the modified Clauser chart method is $\pm 4\,\%$. The uncertainty in U_τ determined using the total stress method is $\pm 5\,\%$. Uncertainties for higher-order statistics are presented with the reduced data.

4. Results

4.1. *Mean flow*

The mean velocity profiles for the rough-wall boundary layers in inner variables are shown in figure 3. The effect of increasing Reynolds number is seen as an increase in the downward shift in the overlap region of the profiles termed the roughness function, ΔU^+. Otherwise, the profiles retain a similar shape. In the present study, the log-law constants of $\kappa = 0.421$ and $B = 5.60$ suggested by McKeon *et al.* (2004) were employed so that direct comparison of the present roughness function results could be made with the rough-wall pipe-flow study of Shockling *et al.* (2006). This study employed these constants and tested a roughness similar to that used in the present study. When the present data were analysed using the constants of Coles (1962), the differences in the friction velocities obtained were well within the experimental uncertainty of the measurements.

More effective comparisons of rough- and smooth-wall boundary layers may be made with the mean profiles plotted in velocity-defect form (figure 4). The agreement between the rough- and smooth-wall profiles is excellent. However, since changes to
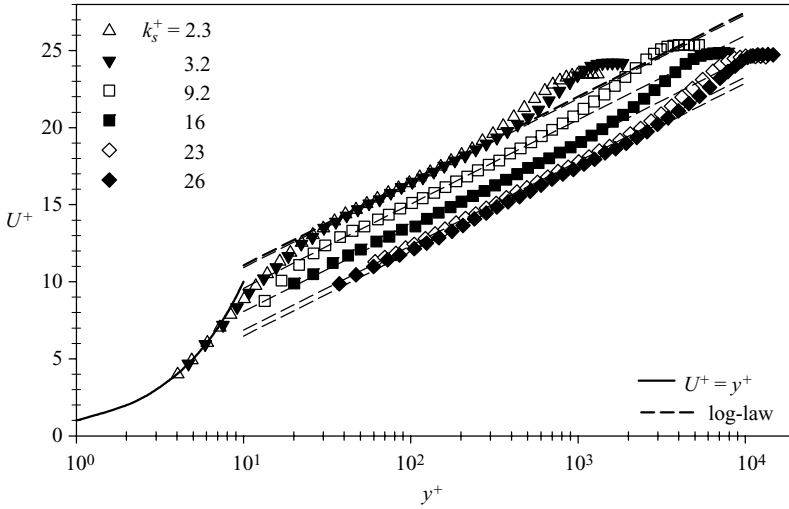
FIGURE 3. Rough-wall mean velocity profiles in inner variables, log constants of
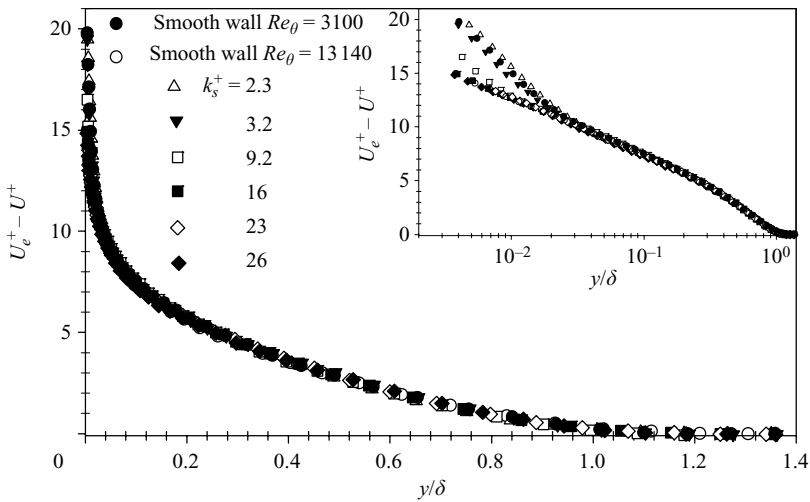McKeon *et al.* (2004), uncertainty in $U^+ = \pm 4$ %.

FIGURE 4. Mean velocity profiles in velocity-defect form for both smooth and rough walls:
inset in log-normal axes, uncertainty in $U_e^+ - U^+ = \pm 4$ %.

the wake are somewhat masked using linear axes, the inset in figure 4 presents the
velocity-defect profiles with log-normal axes. Plotted in this way, differences in the
wake strength, Π, would be observed as a lack of collapse of the profiles in the overlap
region of the boundary layer. An increase in Π for rough-wall boundary layers has
been observed by Krogstad *et al.* (1992), Keirsbulck *et al.* (2002), and Akinlade *et al.*
(2004). Krogstad *et al.* (1992) attributed the increase to the higher growth rate and
greater entrainment of irrotational fluid in the rough-wall boundary layer. However,
this change is not observed in the present velocity-defect profiles. These mean flow
results provide support for Townsend's (1976) Reynolds-number similarity hypothesis
and the proposal of a universal defect profile in the overlap and outer region for zero
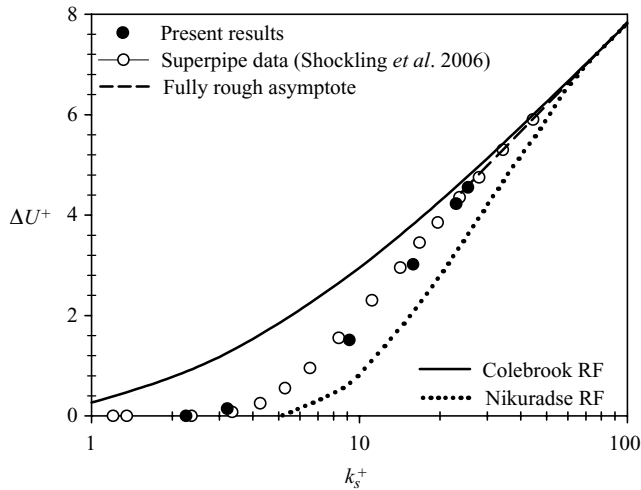pressure gradient boundary layers as proposed by Clauser (1954) and Hama (1954),

FIGURE 5. Roughness function results, ΔU^+ determined using the log constants of McKeon *et al.* (2004), uncertainty in $\Delta U^+ = \pm 10\%$ or 0.2, whichever is larger.

provided that k/δ is small. Similar evidence has been given by Shockling *et al.* (2006) and Krogstad *et al.* (2005), for pipe and turbulent channel flows, respectively.

The roughness function results, ΔU^+, for the rough-wall profiles are presented in figure 5. Shown for comparison, are the rough-wall pipe-flow results of Shockling *et al.* (2006) that were obtained for a geometrically similar roughness. The agreement in the two data sets is excellent. This is in concurrence with the findings of Schultz & Myers (2003) that showed that roughness functions for a given roughness obtained through disparate means yield similar results. In that study, the overall frictional drag on a flat plate, the local mean velocity profile in a turbulent boundary layer, and the overall torque on a rotating disk were used to find the roughness function for several rough surfaces, and the results showed good agreement. It should be noted that both in the present boundary-layer study and the pipe-flow experiments of Shockling *et al.* (2006), the relative roughness height, or ratio of the roughness height to the thickness of the shear layer, is much smaller than previous roughness studies. The value of k_{rms}/R, where R is the pipe radius, was 3.9×10^{-5} in the Shockling study and $k_{rms}/\delta \leqslant 1.0 \times 10^{-3}$ in this work. Jiménez (2004) notes that such studies are critical in order to assess the validity of wall similarity since the approach of most workers has been to use a large relative roughness in order to achieve fully rough flow.

At low roughness Reynolds numbers ($k_s^+ < 2.5$), the present results show that the rough surface is hydraulically smooth ($\Delta U^+ \sim 0$). As the roughness Reynolds number increases, departure from smooth behaviour is observed. Shown for comparison are the Colebrook roughness function (Colebrook 1939) given by Hama (1954) with the log-constants of McKeon *et al.* (2004) and the Nikuradse (1933) roughness function for uniform sand. While the present roughness does not strictly follow either roughness function, it clearly does not display Colebrook-type monotonic behaviour of the roughness function in the transitional regime. Instead, the surface displays Nikuradse-type behaviour, tending toward the hydraulically smooth flow regime at finite k_s^+ with slight inflectional behaviour in the transitional regime. At larger values of k_s^+, the flow reaches the fully rough regime in which the velocity is independent of viscosity, and U_e^+ is constant. The value of U_e^+ in the present study is 24.6 and 24.7

at $k_s^+ = 23$ and 26, respectively. In the fully rough regime, the roughness function is given by

$$\Delta U^+ = \frac{1}{\kappa} \ln k_s^+ + B - B_{FR}' \qquad (4.1)$$

where B_{FR}', the Nikuradse roughness function, in the fully rough flow regime is 8.5 (Nikuradse 1933). The present results show that at the highest roughness Reynolds number tested ($k_s^+ = 26$), the roughness function lies on the fully rough asymptote (equation (4.1)), indicating the boundary layer has reached the fully rough flow regime. Further evidence of fully rough behaviour can also be seen in the profiles of the near-wall streamwise Reynolds normal stress which will be presented later. Nikuradse noted that the fully rough regime exists for $k_s^+ \geqslant 70$ for monodisperse close-packed sandgrain roughness. However, the roughness Reynolds number signifying both the onset of roughness effects ($k_{s,smooth}^+$) and the beginning of the fully rough regime ($k_{s,rough}^+$) depends strongly on the roughness type and uniformity as was noted by Ligrani & Moffat (1986). Their rough surface, consisting of uniform close-packed spheres, displayed a fairly narrow transitionally rough regime with $k_{s,smooth}^+ \approx 15$ and $k_{s,rough}^+ \approx 55$, while the monodisperse close-packed sandgrains of Nikuradse (1933), which was not as uniform, had a wider transitionally rough regime, with $k_{s,smooth}^+ \approx 5$ and $k_{s,rough}^+ \approx 70$. For the present roughness, the results indicate that $k_{s,smooth}^+ \approx 2.5$ and $k_{s,rough}^+ \approx 25$ define the range of the transitionally rough regime. These values are in reasonable agreement with the results of Shockling *et al.* (2006) that showed $k_{s,smooth}^+ \approx 3.5$ and $k_{s,rough}^+ \approx 30$ for a geometrically similar roughness.

Snyder & Castro (2002) also noted the difficulties in defining the onset of the fully rough regime for disparate roughness types. In their study, they adopted the log-law form used in meteorology, given as

$$U^+ = \frac{1}{\kappa} \ln \left(\frac{y}{y_0} \right), \qquad (4.2)$$

where y_0 is a roughness length scale. They point out that while it is commonly held that $y_0^+ > 2$ is necessary for fully rough flow, it depends strongly on the roughness type. They found that for roughness consisting of isolated bluff bodies, the onset of the fully rough condition occurs at y_0^+ closer to 0.5. The highest value of y_0^+ reached in the present study was 0.64.

4.2. *Reynolds stresses*

The streamwise Reynolds normal stress ($\overline{u'^2}^+$) profiles for the smooth and rough surfaces are presented in figure 6 using inner scaling. For the lowest roughness Reynolds numbers ($k_s^+ = 2.3$, 3.2 and 9.2), a near-wall peak at $y^+ \approx 15$ is observed which is similar to that observed on the smooth wall. As k_s^+ increases toward the fully rough flow regime, the rise in $\overline{u'^2}^+$, which is seen to begin at $y^+ \approx 100$ on the smooth wall, is reduced until at $k_s^+ = 26$, it is completely absent. At $k_s^+ = 26$, there is a large plateau region in $\overline{u'^2}^+$ in the outer layer which drops as the wall is approached. The absence of the near-wall rise in $\overline{u'^2}^+$ was shown by Ligrani & Moffat (1986) to be a sensitive indicator of a boundary layer reaching the fully rough regime. The peak in the streamwise Reynolds normal stress on a smooth wall is primarily due to viscous effects and is associated with streamwise vortical structures (Grass 1971). The reduction in the peak is due to the breakup of streamwise vortices by the roughness elements that extend further and further from the wall (in wall variables) as the Reynolds number increases. When the boundary layer reaches the fully rough
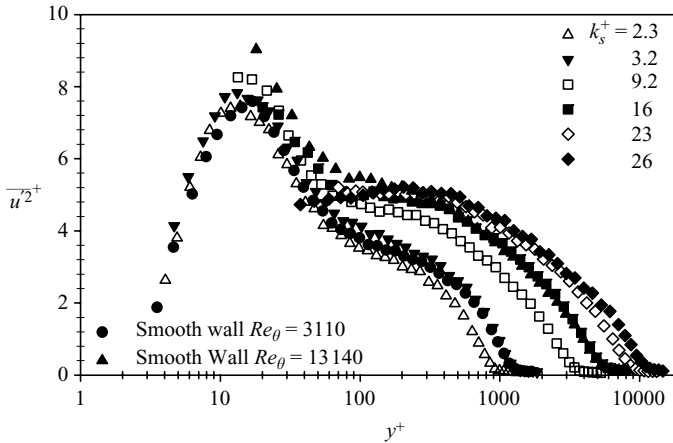
FIGURE 6. Streamwise Reynolds normal stress profiles for all surfaces in inner variables; uncertainty in $\overline{u'^2}^+ = \pm 8\,\%$.
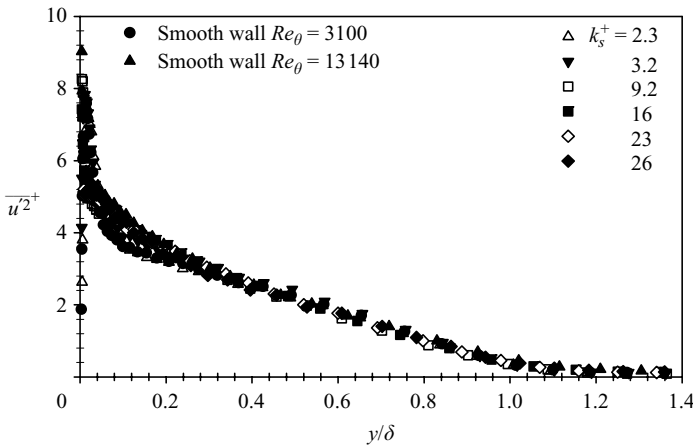

FIGURE 7. Streamwise Reynolds normal stress profiles in outer variables; uncertainty in $\overline{u'^2}^+ = \pm 8\,\%$.

regime, the frictional drag of the wall is dominated by the form drag of the roughness elements and viscous effects become negligible even very near the wall.

Figure 7 shows the profiles of $\overline{u'^2}^+$ for the smooth and rough surfaces in outer scaling. Reynolds-number dependence in the overlap region can be observed for both the smooth- and rough-wall cases. This is seen as a slight increase in $\overline{u'^2}^+$ with Reynolds number. There is, however, good agreement of the smooth- and rough-wall results in the overlap and outer region of the boundary layer when similar Reynolds-number cases are compared. This similarity in the streamwise Reynolds normal stress for rough and smooth walls in the outer flow is fairly well accepted and has been observed in previous roughness studies (see Raupach *et al.* 1991; Jiménez 2004). Likewise, the present streamwise Reynolds normal stress profiles provide support for the concept of wall similarity. It should also be noted that all the present smooth-wall Reynolds-stress profiles agree well with those of DeGraaff & Eaton (2000) at similar Reynolds numbers.
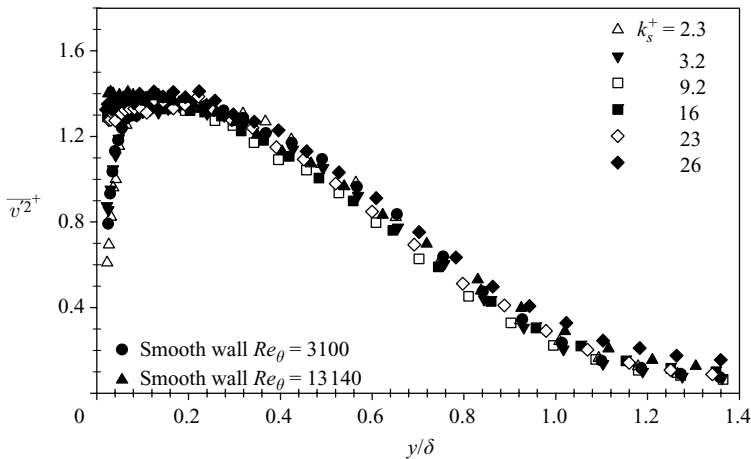
FIGURE 8. Wall-normal Reynolds normal stress profiles for all surfaces
in outer scaling; uncertainty in $\overline{v'^2}^+ = \pm 9$ %.

Figure 8 shows the profiles of $\overline{v'^2}^+$ for the smooth and rough surfaces in outer scaling. The agreement of the smooth and rough profiles is within the experimental uncertainty of the measurements across the overlap and outer regions of the boundary layer. For both the smooth- and rough-wall profiles, a rather broad plateau of $\overline{v'^2}^+ \approx 1.3$–$1.4$ is observed in the overlap region. This is in agreement with DeGraaff & Eaton (2000), who observed a plateau in $\overline{v'^2}^+ \approx 1.35$ for smooth walls at $Re_\theta \geqslant 2900$. The effect of roughness on the wall-normal or 'active' turbulent motions has been the topic of considerable debate. Raupach *et al.* (1991), based on the roughness literature to date, concluded that there was similarity in $\overline{v'^2}^+$ outside the roughness (or viscous) sublayer for rough and smooth walls. Since that time, there has been work that supports this view (e.g. Flack *et al.* 2005; Kunkel & Marusic 2006) and work that shows that roughness effects on the wall-normal component extend well into the outer layer (e.g. Krogstad *et al.* 1992; Leonardi *et al.* 2003). Jiménez (2004) tried to reconcile these conflicting views by concluding that the differences might be the effect of the relative roughness, k/δ, on the flow. He noted that in cases in which the relative roughness is large ($k/\delta \gtrsim 1/50$), the roughness effect on the wall-normal component may be observed well into the outer layer. There appear to be other possibilities, however. A case in point is the DNS and experimental study of Krogstad *et al.* (2005) on channels roughened by transverse bars. In this study, results of both the DNS and the experiment showed little effect of the roughness on $\overline{v'^2}^+$ outside the roughness sublayer. The boundary-layer study of Krogstad & Antonia (1999) that used two-dimensional transverse rods found that $\overline{v'^2}^+$ was increased significantly, well into the outer layer. This led Krogstad *et al.* (2005) to hypothesize that the internal flows such as channel and pipe flows may respond differently to roughness than do boundary-layer flows. Further study is required to see if this is indeed the case. Nonetheless, the present $\overline{v'^2}^+$ profiles provide support for the concept of wall similarity for boundary layers in which the relative roughness is small and the Reynolds number is large.

The $-\overline{u'v'}^+$ profiles for the smooth and rough surfaces in outer scaling are shown in figure 9. Again, there is no significant difference in the smooth- and rough-wall
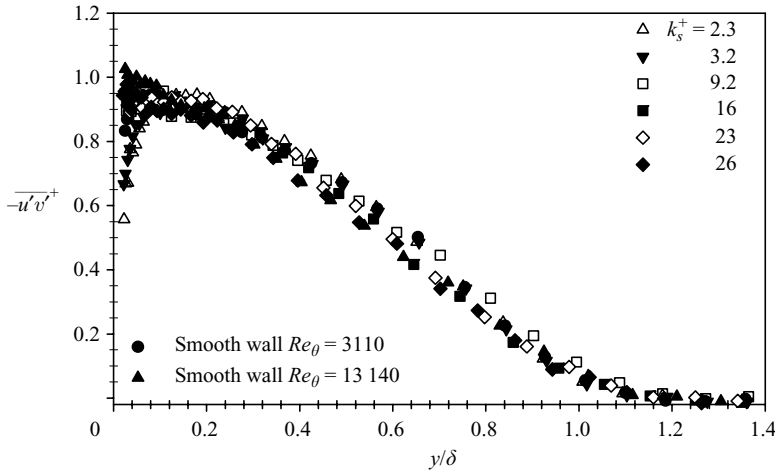
FIGURE 9. Reynolds shear stress profiles for all surfaces in outer scaling;
uncertainty in $-\overline{u'v'}^+ = \pm 9\,\%$.

profiles in the outer part of the boundary layer. Krogstad *et al.* (1992) observed a moderate increase in $-\overline{u'v'}^+$ for a woven mesh roughness compared to a smooth wall in the outer layer. However, the difference was smaller than was seen in $\overline{v'^2}^+$. The differences in $\overline{v'^2}^+$ and $-\overline{u'v'}^+$ were attributed in part to the less strict wall boundary condition for the wall-normal velocity component on a rough surface compared to a smooth one. For example, on a smooth wall, the wall-normal velocity fluctuations must go to zero at $y = 0$. On a rough wall, $y = 0$ is located between the roughness peaks and troughs, not strictly on the wall, so the wall-normal velocity fluctuations may be non-zero there. Also, the type of roughness would seem to play a major role in the severity of this boundary condition. Woven mesh and transverse bars, for example, provide more 'porosity' to the wall-normal motions than close-packed three-dimensional roughness like sand roughness and the surface used in the present study. However, Flack *et al.* (2005) found little change in the Reynolds stresses over woven mesh for $y > 3k_s$.

4.3. *Quadrant decomposition*

Quadrant decomposition (Wallace, Eckelmann & Brodkey 1972) was used in order to examine possible changes in turbulence structure resulting from the surface roughness. The technique sorts turbulent events into each of the four quadrants of the (u', v')-plane providing information regarding the turbulence structure. In particular, it allows the contributions of ejection ($Q2$) and sweep ($Q4$) motions to the total Reynolds shear stress to be calculated. In the present work, the quadrant decomposition was carried out using the hyperbolic hole size (H) method of Lu & Willmarth (1973).

The contribution to $\overline{u'v'}$ from a given quadrant, Q, can be expressed as

$$(\overline{u'v'})_Q = \lim_{T \to \infty} \frac{1}{T} \int_0^T u'v'(t) I_Q(t)\,\mathrm{d}t, \qquad (4.3)$$

where $I_Q(t)$ is a trigger function defined as

$$I_Q = \begin{cases} 1 & \text{when } |u'v'|_Q \geqslant H(\overline{u'^2})^{1/2}(\overline{v'^2})^{1/2}, \\ 0 & \text{otherwise}. \end{cases} \qquad (4.4)$$
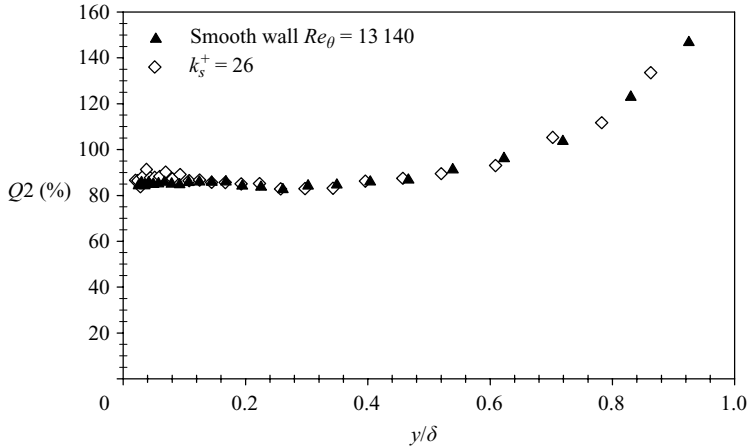
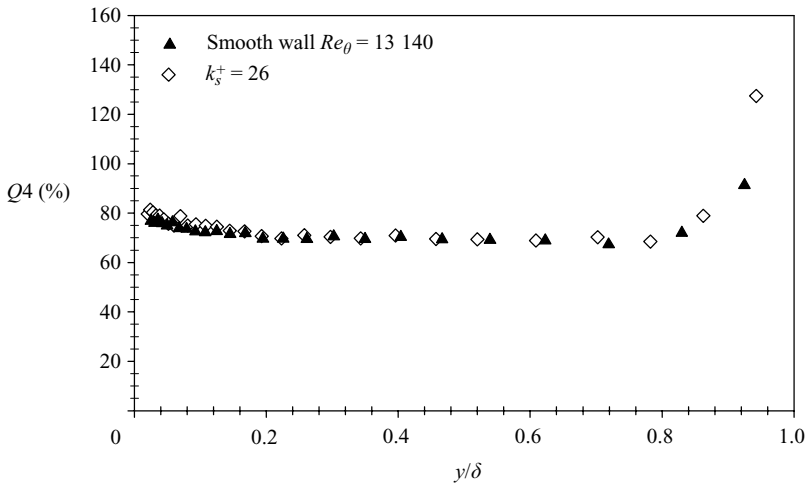FIGURE 10. Percentage contribution to the Reynolds shear stress from $Q2$ events ($H = 0$).

FIGURE 11. Percentage contribution to the Reynolds shear stress from $Q4$ events ($H = 0$).

Figures 10 and 11 show the percentage contributions from ejection and sweep events, respectively, to the Reynolds shear stress for $H = 0$. It should be noted that for clarity only the highest-Reynolds-number cases for the smooth and rough wall are presented for the quadrant decomposition. However, the trends were very similar for the lower-Reynolds-number cases.

The present results show that there is excellent agreement in the contributions from both $Q2$ and $Q4$ events for the smooth- and rough-wall boundary layers. This is in agreement with previous work (Flack *et al.* 2005) which showed similar results for both sandpaper and woven mesh roughness. The relative roughness height, k_s/δ, in that study was $1/62$ and $1/45$ for the sandpaper and mesh roughness, respectively. The ratio k_s/δ for the rough-wall results presented here is $1/400$. In contrast, Krogstad *et al.* (1992) observed a significant increase in $(-\overline{u'v'})_2^+$ across much of the boundary layer for a woven mesh roughness compared to a smooth wall with $H = 0$. An increase in $(-\overline{u'v'})_4^+$ in the wall region was also noted. The ratio k_s/δ was $1/15$ in that study.
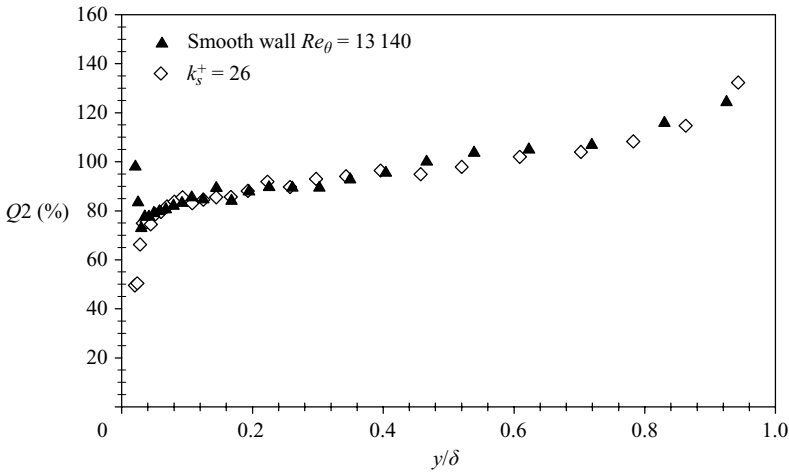
FIGURE 12. Percentage contribution to the conditionally averaged Reynolds shear stress from $Q2$ events ($H = 2$).
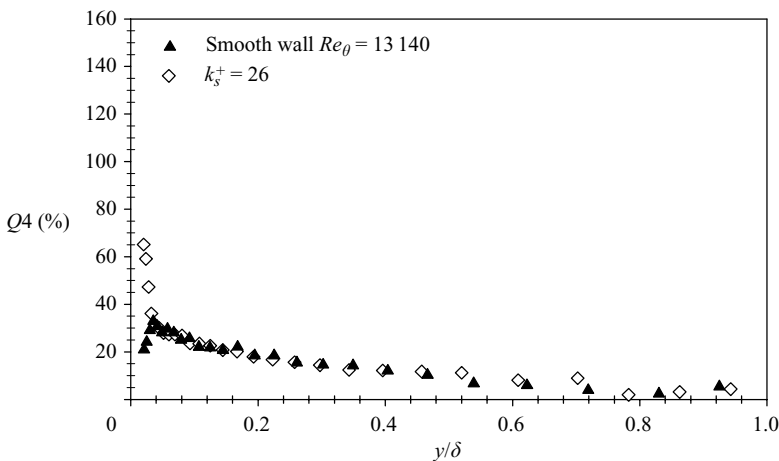

FIGURE 13. Percentage contribution to the conditionally averaged Reynolds shear stress from $Q4$ events ($H = 2$).

The differences observed among these studies may be a result of differences in scale separation between the roughness length scale and the largest turbulence scales in the flow. Jiménez (2004) hypothesized that if the scale separation is insufficient, roughness effects may be observed well into the outer flow. The scale separation in the present study is extremely large, typified by the extremely small value of the relative roughness k_s/δ. The degree of scale separation in the present work is much larger than achieved in any previous laboratory boundary-layer study able to reach the fully rough flow regime.

Figures 12 and 13 show the percentage contributions from ejection and sweep events, respectively, to the conditionally averaged Reynolds shear stress for $H = 2$. Using $H = 2$ isolates strong turbulence events in which the instantaneous Reynolds shear stress is larger in magnitude than $5\overline{u'v'}$.
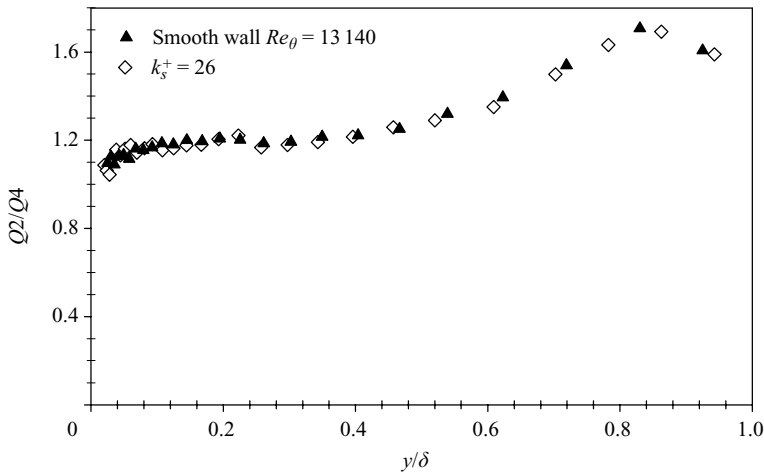
FIGURE 14. Ratio of $Q2$ to $Q4$ events ($H = 0$).

Again, the results show good agreement in the contributions from both $Q2$ and $Q4$ events for the smooth- and rough-wall boundary layers across most of the boundary layer. However, near the wall ($y/\delta \leqslant 0.025$), the percentage contribution from strong ejection events on the rough wall decreases, while the percentage contribution from strong sweep events increases. In contrast, near the smooth wall, the contribution from strong ejection events increases, while the percentage contribution from strong sweep events decreases. These differences observed in the near-wall region between the rough and smooth walls are in agreement with the results of Krogstad *et al.* (1992) and Flack *et al.* (2005) for woven mesh and sandpaper roughness. Krogstad & Antonia (1999) observed a similar trend for a transverse rod roughness with the effect persisting well into the outer flow. The relative roughness, k_s/δ, was 1/8 in that study. In the present investigation in which the relative roughness is much smaller, the differences between the rough and smooth wall are confined to the near-wall region. It should be noted that for the smooth wall, $y/\delta = 0.025$ corresponds to $y^+ = 119$, and for the rough wall, it corresponds to $y^+ = 253$ or $y \approx 10k_s$. Therefore, the differences observed for $y/\delta \leqslant 0.025$ could either be the direct influence of the roughness on the turbulence structure or simply the lack of viscous influence on the rough wall, which is increasingly important on the smooth wall in this region.

In order to highlight the relative importance of ejection and sweep events to the maintenance of the Reynolds shear stress, the ratios of the $Q2$ to $Q4$ contributions are presented in figures 14 and 15 for $H = 0$ and $H = 2$, respectively. For $H = 0$, the agreement between the rough- and smooth-wall results is quite good throughout the entire boundary layer.

The profiles of $Q2/Q4$ for the strong Reynolds stress events ($H = 2$) show good agreement across most of the boundary layer (figure 15). However, some changes are observed in the near-wall region ($y/\delta \leqslant 0.025$). For the smooth wall, $Q2/Q4$ maintains a value greater than 2 throughout the boundary layer, and the ratio increases as the wall is approached. This illustrates the relative importance of strong ejection events compared to strong sweeps on a smooth surface, especially very close to the wall. On the rough wall, $Q2/Q4$ is also greater than 2 for most of the boundary layer. However, $Q2/Q4$ is observed to decrease to a value of less than unity as the wall is approached. This indicates that near the roughness, strong sweeps actually make
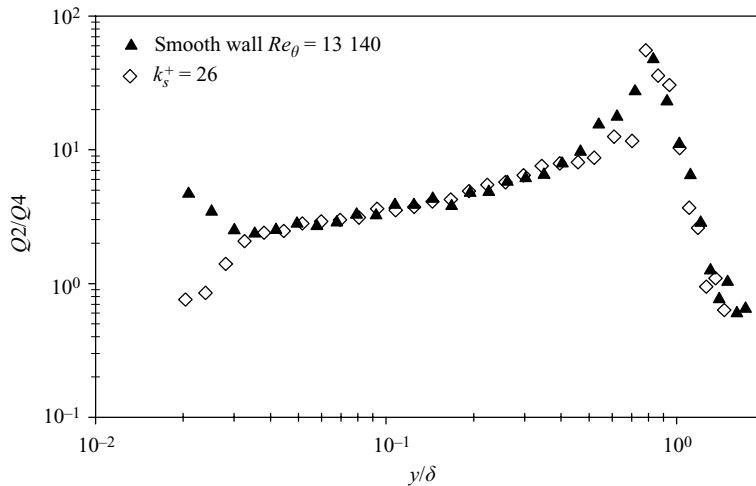
FIGURE 15. Ratio of $Q2$ to $Q4$ events ($H = 2$).

a larger contribution to the Reynolds shear stress than do ejections. This is in accordance with the studies of Krogstad *et al.* (1992) and Flack *et al.* (2005) which both showed similar changes close to a rough wall. The differences in the relative importance of strong ejection and sweep events are believed to be the result of the less strict wall-boundary condition for the wall-normal velocity component on a rough surface compared to a smooth one. It should be noted that these differences are confined to the near-wall region in the present study.

4.4. *Higher-order turbulence statistics*

While the present results in terms of the mean flow, Reynolds stresses, and quadrant decomposition of the Reynolds shear stress indicate that roughness effects are confined to the near-wall region, the velocity triple products will now be examined. Andreopoulos & Bradshaw (1981) showed these quantities to be an indicator of changes in turbulence structure due to the surface boundary condition. As with the quadrant decomposition, only the highest-Reynolds-number cases for the smooth and rough wall are presented for the velocity triple products. Murlis, Tsai & Bradshaw (1982) noted that these quantities display only a weak Reynolds-number dependence even at $Re_\theta < 5000$ in the outer flow. For both the present cases shown, the Reynolds number is much higher ($Re_\theta > 13\,000$). It is believed, therefore, that a valid assessment of the effect of roughness on the triple products can be made, despite the difference in Reynolds number between the smooth and rough cases. Profiles of the velocity triple product $\overline{u'^3}^+$ for the smooth and rough wall are shown in figure 16. Over most of the boundary layer, the agreement between the rough and smooth wall is quite good. Near the wall at $y/\delta \leqslant 0.025$, some significant differences are noted (see inset in figure 16). On the rough wall, $\overline{u'^3}^+$ changes sign and becomes positive near the roughness. For the smooth wall, it remains negative across the entire boundary layer. This difference may be due to changes in the ejection-sweep cycle and modification of the longitudinal vortices and accompanying low-speed streaks by the roughness. The flow visualizations by Grass (1971) showed that while ejection-sweep cycle over rough and smooth walls exhibited a high degree of similarity, the particulars of the mechanics of the entrainment of low momentum fluid at the wall differed. One notable difference was a relative lack of long streamwise vortices near the rough wall.
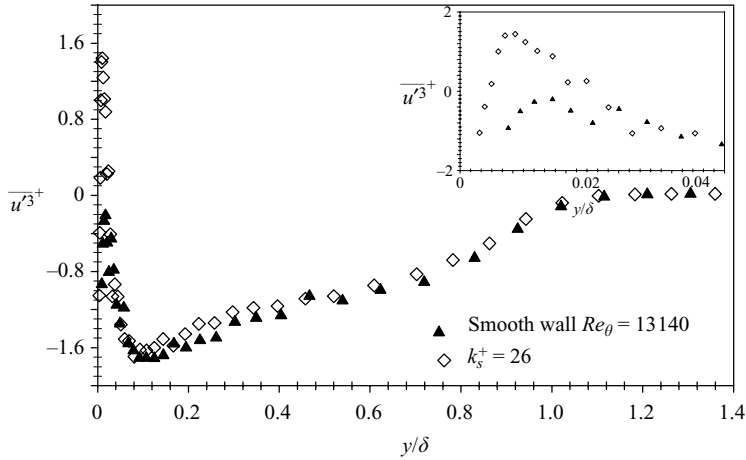
FIGURE 16. The velocity triple product $\overline{u'^3}^+$ for highest-Reynolds-number smooth and rough walls in outer scaling; near-wall region shown in inset; uncertainty in $\overline{u'^3}^+ = \pm 16\,\%$.
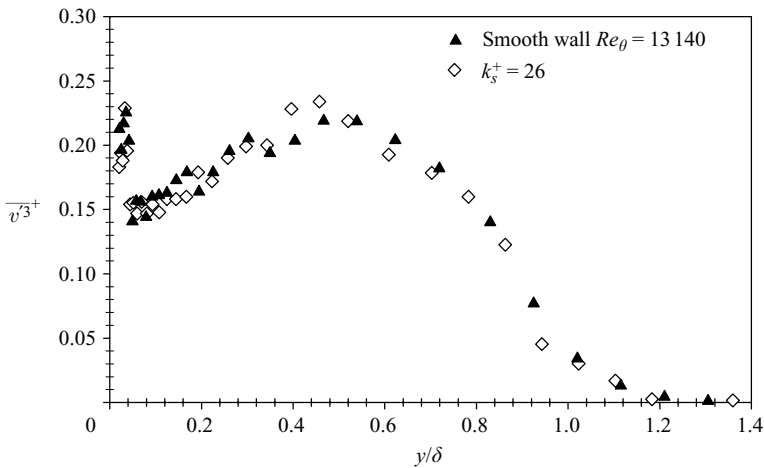

FIGURE 17. The velocity triple product $\overline{v'^3}^+$ for highest-Reynolds-number smooth and rough walls in outer scaling; uncertainty in $\overline{v'^3}^+ = \pm 25\,\%$.

The modifications to these vortices by the roughness are probably involved in the changes observed in $\overline{u'^3}^+$ as well as destruction of the peak in $\overline{u'^2}^+$ when the flow is fully rough.

The distributions of the velocity triple product $\overline{v'^3}^+$ are presented in figure 17. The present smooth- and rough-wall results agree within their uncertainty throughout the boundary layer. Antonia & Krogstad (2001) showed that the profile of $\overline{v'^3}^+$ was considerably altered for flows over transverse rods. They observed that the value of $\overline{v'^3}^+$ was negative over a significant fraction of the boundary layer while this triple product remained positive for a smooth and a woven mesh roughness over the entire layer. This observation on the two-dimensional, transverse rod roughness indicates that the direction of transport of v'^2 turbulent kinetic energy (TKE) is toward the wall, not away from it as is observed for smooth walls and the present roughness.
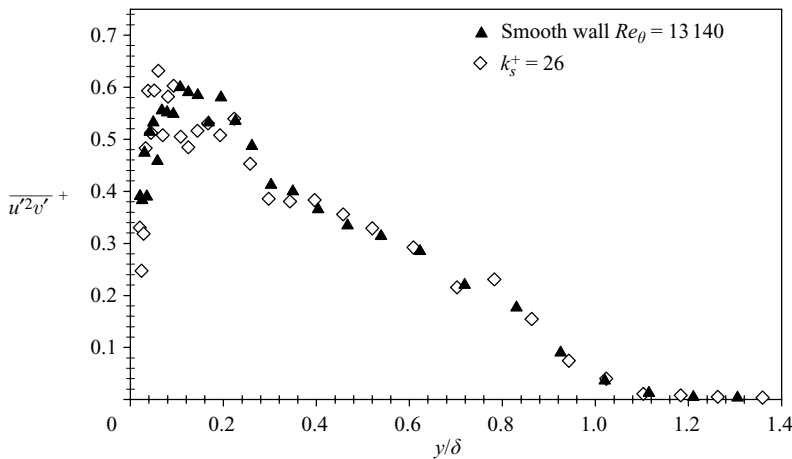
FIGURE 18. The velocity triple product $\overline{u'^2 v'}^+$ for highest-Reynolds-number smooth and rough walls in outer scaling; uncertainty in $\overline{u'^2 v'}^+ = \pm 17\,\%$.

It should be noted that the relative roughness, k_s/δ was $1/8$ for the transverse rods of Antonia & Krogstad (2001), which is quite large. However, it is not clear if the differences observed are due to this or more fundamental differences in the flows over two- and three-dimensional roughness. Bandyopadhyay & Watson (1988) observed similar differences in the velocity triple products between two- and three-dimensional roughness.

The results for the velocity triple product $\overline{u'^2 v'}^+$ are shown in figure 18. This term represents the wall-normal transport of the u'^2 contribution to the TKE by the v' fluctuations. The present results show good similarity in $\overline{u'^2 v'}^+$ for smooth and rough walls in the outer flow. Closer to the wall, the results are more scattered, but the differences observed are within the experimental uncertainty of the measurements. Flack *et al.* (2005) noted that $\overline{u'^2 v'}^+$ was significantly reduced close to a rough wall ($y < 5k_s$). However, the closest point to the wall for the v'-based triple products presented here is $y \approx 8k_s$, which is outside the zone they showed to be influenced by the roughness. Antonia & Krogstad (2001) observed that $\overline{u'^2 v'}^+$ was negative over a significant fraction of the boundary layer for a two-dimensional transverse rod roughness, indicating transport of TKE toward the wall instead of away from it. They also noted differences in the behaviour of the gradients $\partial \overline{u'^2 v'}/\partial y$ and $\partial \overline{v'^3}/\partial y$ for two- and three-dimensional roughness near the wall. This gradient reflects the turbulent diffusion of u'^2 and v'^2 TKE by the v' fluctuations. For a two-dimensional roughness, they observed a negative gradient signifying a gain in TKE, whereas for a three-dimensional roughness there was a loss of TKE by turbulent diffusion.

The profiles of the velocity triple product $\overline{u'v'^2}^+$ are shown in figure 19. This triple product represents the wall-normal turbulent flux of the Reynolds shear stress. Although there is some scatter in the present results, there are no striking differences observed between the smooth- and rough-wall profiles over most of the boundary layer. Previous work by the present authors (Flack *et al.* 2005) also showed good agreement in $\overline{u'v'^2}^+$ for rough- and smooth-wall boundary layers over much of the boundary layer. However, for both the sandpaper and woven mesh roughness that were tested, $\overline{u'v'^2}^+$ became positive near the wall ($y < 5k_s$), indicating a flux of Reynolds shear stress toward the surface as opposed to away from it, as is observed here. This change in
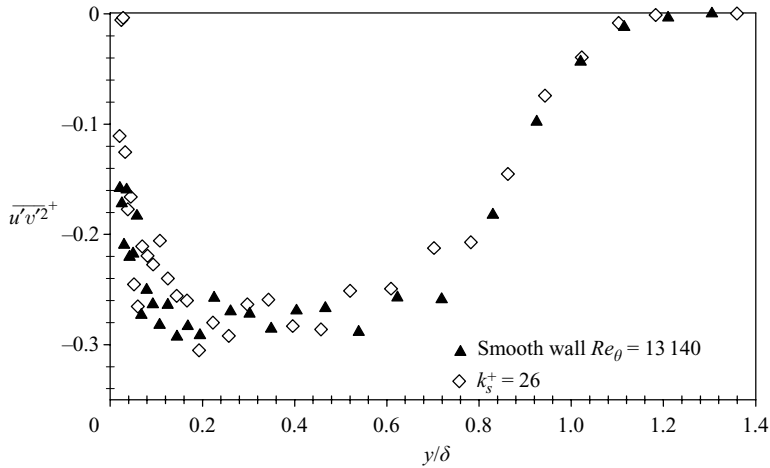
FIGURE 19. The velocity triple product $\overline{u'v'^2}^+$ for highest-Reynolds-number smooth and rough walls in outer scaling; uncertainty in $\overline{u'v'^2}^+ = \pm 19\,\%$.

near-wall transport was also noted by Andreopoulos & Bradshaw (1981). Again, since the closest point to the wall for the v'-based triple products presented here is $y \approx 8k_s$, the change in near-wall transport cannot be directly corroborated by the present results. However, some differences are observed for $y/\delta \leqslant 0.025$ ($y \approx 10k_s$) with the rough-wall $\overline{u'v'^2}^+$ approaching zero whereas the smooth-wall $\overline{u'v'^2}^+$ remains negative.

5. Conclusions

Experimental measurements that cover a wide Reynolds-number range, spanning the hydraulically smooth to the fully rough flow regime for a single surface with a small relative roughness height, have been presented and compared to those for a smooth wall. The rough-wall experiments were made on a three-dimensional rough surface geometrically similar to the honed pipe roughness used by Shockling *et al.* (2006) in the Princeton superpipe facility. The roughness functions (ΔU^+) for the present boundary-layer tests show good agreement with the superpipe results and indicate that a three-dimensional roughness with a nearly Gaussian distribution shows inflectional behaviour and does not follow a monotonic Colebrook-type roughness function (Colebrook 1939) as suggested by the Moody diagram (1944).

The present results for the mean flow, Reynolds stresses, quadrant decomposition of the Reynolds shear stress, and turbulent transport of the Reynolds stresses (velocity triple products) all show excellent agreement between rough- and smooth-wall boundary layers in the overlap and outer regions, and, therefore, provide compelling support for the wall similarity hypothesis (Townsend 1976; Raupach *et al.* 1991). These results indicate that if the separation of scales between the roughness and the largest turbulent length scales is sufficient, the outer layer is independent of surface condition except for the role that the wall conditions have on setting the length (δ) and velocity (U_τ) boundary conditions for the outer flow. This is not to say that roughness has no effect on the flow. Differences in the turbulence were observed in the near-wall region of the boundary layer ($y/\delta \leqslant 0.025$ or $y \leqslant 10k_s$). For example, the near-wall peak in $\overline{u'^2}^+$ is observed to be reduced with increasing k_s^+, which was also noted by Ligrani & Moffat (1986) in turbulent boundary-layer flow and Krogstad *et al.* (2005)

in turbulent channel flow. This is probably due to the roughness modification of the viscous-influenced coherent structures that give rise to the peak on a smooth wall (e.g. near-wall longitudinal vortices and low-speed streaks). Quadrant decomposition also shows that there is an increase in strong sweep events and a decrease in strong ejection events near the rough wall. However, outside the near-wall region, the mean flow and turbulence properties appear to be independent of the surface condition.

Despite the significant amount of work that has focused on roughness effects on wall-bounded shear flows, the picture is still not clear on the range of validity of the wall similarity hypothesis. It seems reasonable, as Jiménez (2004) contends, that the outer flow may be directly affected by the roughness if there is not sufficient scale separation between the roughness height and the boundary-layer thickness. However, there also seem to be some trends regarding roughness type which emerge from the literature. The most significant changes to the outer flow appear to occur with two-dimensional roughness, such as transverse rods (e.g. Krogstad & Antonia 1999) and bars (e.g. Leonardi *et al.* 2003). Three-dimensional roughness such as closely packed spheres (e.g. Ligrani & Moffat 1986), sandpaper (e.g. Flack *et al.* 2005), and sanded surfaces (e.g. Schultz & Flack 2003) tend to show much less effect on the outer flow. Other roughness types, such as three-dimensional woven mesh, have been used to both support (Flack *et al.* 2005) and dispute (Krogstad *et al.* 1992) the concept of wall similarity. A common thread in roughness types that show effects in the outer layer is the relative large ΔU^+ they produce for their maximum peak-to-trough height (k_T). This can be quantified by the ratio k_s/k_T. For most close-packed three-dimensional roughness, $k_s/k_T \leqslant \sim 1$. For two-dimensional transverse rods, the ratio k_s/k_T may be greater than 6 (Krogstad & Antonia 1999). Additional work is necessary to understand the effects of large relative roughness and the difference between roughness types. The present study has shown that in the limit of high Reynolds number with a small relative roughness height, turbulence effects are limited to the near-wall region, supporting the wall similarity hypothesis.

REFERENCES

ADRIAN, R. J. 1983 Laser velocimetry. In *Fluid Mechanics Measurements* (ed. R. J. Goldstein). Hemisphere.

AKINLADE, O. G., BERGSTROM, D. J., TACHIE, M. F. & CASTILLO, L. 2004 Outer flow scaling of smooth and rough wall turbulent boundary layers. *Exps. Fluids* **37**, 604–612.

ANDREOPOULOS, J. & BRADSHAW, P. 1981 Measurements of turbulence structure in the boundary layer on a rough surface. *Boundary-Layer Met.* **20**, 201–213.

ANTONIA, R. A. & KROGSTAD, P.-Å. 2001 Turbulence structure in boundary layers over different types of surface roughness. *Fluid Dyn. Res.* **28**, 139–157.

ANTONIA, R. A. & LUXTON, R. E. 1971 The response of a turbulent boundary layer to a step change in surface roughness. Part 1. Smooth to rough. *J. Fluid Mech.* **48**, 721–761.

BANDYOPADHYAY, P. R. 1987 Rough-wall turbulent boundary layers in the transition regime. *J. Fluid Mech.* **180**, 231–266.

BANDYOPADHYAY, P. R. & WATSON, R. D. 1988 Structure of rough-wall boundary layers. *Phys. Fluids* **31**, 1877–1883.

BHAGANAGAR, K., KIM, J. & COLEMAN, G. 2004 Effect of roughness on wall-bounded turbulence. *Flow Turbulence Combust.* **72**, 463–492.

BUCHHAVE, P., GEORGE, W. K. & LUMLEY, J. L. 1979 The measurement of turbulence with the laser-Doppler anemometer. *Annu. Rev. Fluid Mech.* **11**, 443–503.

CLAUSER, F. H. 1954 Turbulent boundary layers in adverse pressure gradients. *J. Aeronaut. Sci.* **21**, 91–108.

COLEBROOK, C. F. 1939 Turbulent flow in pipes, with particular reference to the transitional region between smooth and rough wall laws. *J. Inst. Civil Engrs* **11**, 133–156.

COLEBROOK, C. F. & WHITE, C. M. 1937 Experiments with fluid friction in roughened pipes. *Proc. R. Soc.* **161**, 367–378.

COLEMAN, H. W. & STEELE, W. G. 1995 Engineering application of experimental uncertainty analysis. *AIAA J.* **33**, 1888–1896.

COLES, D. E. 1956 The law of the wake in the turbulent boundary layer. *J. Fluid Mech.* **1**, 191–226.

COLES, D. E. 1962 The turbulent boundary layer in a compressible fluid. *RAND Tech. Rep.* R-403-PR.

DEGRAAFF, D. B. & EATON, J. K. 2000 Reynolds-number scaling of the flat-plate turbulent boundary layer. *J. Fluid Mech.* **422**, 319–346.

DURST, F., FISCHER, M., JOVANOVIC, J. & KIKURA, H. 1998 Methods to set up and investigate low Reynolds number, fully developed turbulent plane channel flows. *Trans. ASME I: J. Fluids Engng* **120**, 496–503.

EDWARDS, R. V. 1987 Report of the special panel on statistical particle bias problems in laser anemometry. *Trans. ASME I: J. Fluids Engng* **109**, 89–93.

EFRON, B. 1982 *The Jackknife, the Bootstrap, and Other Resampling Plans.* 1st edn. Society of Industrial and Applied Mathematics.

FERNHOLZ, H. H. & FINLEY, P. J. 1996 Incompressible zero-pressure-gradient turbulent boundary layer: an assessment of the data. *Prog. Aerospace Sci.* **32**, 245–311.

FLACK, K. A., SCHULTZ, M. P. & SHAPIRO, T. A. 2005 Experimental support for Townsend's Reynolds number similarity hypothesis on rough walls. *Phys. Fluids* **17**, 035102.

GRASS, A. J. 1971 Structural features of turbulent flow over smooth and rough boundaries. *J. Fluid Mech.* **50**, 233–255.

HAMA, F. R. 1954 Boundary-layer characteristics for rough and smooth surfaces. *Trans. SNAME* **62**, 333–351.

JIMÉNEZ, J. 2004 Turbulent flows over rough walls. *Annu. Rev. Fluid Mech.* **36**, 173–196.

JOHANSSON, A. V. & ALFREDSSON, P. H. 1983 Effects of imperfect spatial resolution on measurements of wall bounded turbulent shear flows. *J. Fluid Mech.* **137**, 409–421.

VON KÁRMÁN, T. 1930 Mechanishe aehnlichkeit and turbulenz. *Nachr. Ges. Wiss. Göttingen* 58–76.

KEIRSBULCK, L., LABRAGA, L., MAZOUZ, A. & TOURNIER, C. 2002 Surface roughness effects on turbulent boundary layer structures. *Trans. ASME I: J. Fluids Engng* **124**, 127–135.

KROGSTAD, P.-Å. & ANTONIA, R. A. 1999 Surface roughness effects in turbulent boundary layers. *Exps Fluids* **27**, 450–460.

KROGSTAD, P.-Å., ANTONIA, R. A. & BROWNE, L. W. B. 1992 Comparison between rough- and smooth-wall turbulent boundary layers. *J. Fluid Mech.* **245**, 599–617.

KROGSTAD, P.-Å., ANDERSSON, H. I., BAKKEN, O. M. & ASHRAFIAN, A. 2005 An experimental and numerical study of channel flow with rough walls. *J. Fluid Mech.* **530**, 327–352.

KUNKEL, G. J. & MARUSIC, I. 2006 Study of the near-wall-turbulent region of the high-Reynolds-number boundary layer using an atmospheric flow. *J. Fluid Mech.* **548**, 375–402.

LEONARDI, S., ORLANDI, P., SMALLEY, R. J., DJENIDI, L. & ANTONIA, R. A. 2003 Direct numerical simulations of turbulent channel flow with transverse square bars on one wall. *J. Fluid Mech.* **491**, 229–238.

LIGRANI, P. M. & MOFFAT, R. J. 1986 Structure of transitionally rough and fully rough turbulent boundary layers. *J. Fluid Mech.* **162**, 69–98.

LU, S. S. & WILLMARTH, W. W. 1973 Measurements of the structure of the Reynolds stress in a turbulent boundary layer. *J. Fluid Mech.* **60**, 481–571.

LUCHIK, T. S. & TIEDERMAN, W. G. 1985 Effect of spanwise probe volume length on laser velocimeter measurements in wall bounded turbulent flows. *Exps. Fluids* **3**, 339–341.

MCKEON, B. J., LI, J., JIANG, W., MORRISON, J. F. & SMITS, A. J. 2004 Further observations on the mean velocity distribution in fully developed pipe flow. *J. Fluid Mech.* **501**, 135–147.

MILLIKAN, C. M. 1938 A critical discussion of turbulent flows in channels and circular tubes. *Proc. 5th Intl Congress on Appl. Mech. Cambridge, MA*, pp. 386–392.

MOFFAT, R. J. 1988 Describing the uncertainties in experimental results. *Expl Thermal Fluid Sci.* **1**, 3–17.

MOODY, L. F. 1944 Friction factors for pipe flow. *Trans. ASME* **66**, 671–684.

MURLIS, J., TSAI, H. M. & BRADSHAW, P. 1982 The structure of turbulent boundary layers at low Reynolds numbers. *J. Fluid Mech.* **122**, 13–56.

NIKURADSE, J. 1933 Laws of flow in rough pipes. *NACA TM* 1292.

ÖSTERLUND, J. M., JOHANSSON, A. V., NAGIB, H. M. & HITES, M. H. 2000 A note on the overlap region in turbulent boundary layers. *Phys. Fluids* **12**, 1–4.

PATEL, V. C. 1998 Perspective: flow at high Reynolds number and over rough surfaces – Achilles heel of CFD. *Trans. ASME I: J. Fluids Engng* **120**, 434–444.

PERRY, A. E. & JOUBERT, P. N. 1963 Rough wall boundary layers in adverse pressure gradients. *J. Fluid Mech.* **17**, 193–211.

PERRY, A. E. & LI, J. D. 1990 Experimental support for the attached-eddy hypothesis in zero-pressure gradient turbulent boundary layers. *J. Fluid Mech.* **218**, 405–438.

PERRY, A. E., SCHOFIELD, W. H. & JOUBERT, P. N. 1969 Rough-wall turbulent boundary layers. *J. Fluid Mech.* **37**, 383–413.

RAUPACH, M. R. 1981 Conditional statistics of Reynolds stress in rough-wall and smooth-wall turbulent boundary layers. *J. Fluid Mech.* **108**, 363–382.

RAUPACH, M. R., ANTONIA, R. A. & RAJAGOPALAN, S. 1991 Rough-wall boundary layers. *Appl. Mech. Rev.* **44**, 1–25.

SCHUBAUER, G. B. & TCHEN, C. M. 1961 *Turbulent Flow*. Princeton University Press.

SCHULTZ, M. P. & FLACK, K. A. 2003 Turbulent boundary layers over surfaces smoothed by sanding. *Trans. ASME I: J. Fluids Engng* **125**, 863–870.

SCHULTZ, M. P. & MYERS, A. 2003 Comparison of three roughness function determination methods. *Exps. Fluids* **35**, 372–379.

SHOCKLING, M. A., ALLEN, J. J. & SMITS, A. J. 2006 Roughness effects in turbulent pipe flow. *J. Fluid Mech.* **564**, 267–285.

SNYDER, W. H. & CASTRO, I. P. 2002 The critical Reynolds number for rough-wall boundary layers. *J. Wind Engng Indust. Aerodyn.* **90**, 41–54.

TACHIE, M. F., BERGSTROM, D. J. & BALACHANDAR, R. 2000 Rough wall turbulent boundary layers in shallow open channel flow. *J. Fluids Engng* **122**, 533–541.

TOWNSEND, A. A. 1976 *The Structure of Turbulent Shear Flow*, 2nd edn. Cambridge University Press.

WALLACE, J. M., ECKELMANN, H. & BRODKEY, R. S. 1972 The wall region in turbulent shear flow. *J. Fluid Mech.* **54**, 39–48.

WILLMARTH, W. W. & SHARMA, L. K. 1984 Study of turbulent structure with hot wires smaller than the viscous length. *J. Fluid Mech.* **142**, 121–149.